Research on Engineering Structures & Materials
www.jresm.org
MIM Research Group

Research Article

Experimental and numerical investigation of brick masonry behavior considering mortar joint thickness using an RVE approach

Majid A. Abdulhussein [*,a]

Faculty of Civil Engineering, University of Al-Qadisiyah, Al-Diwaniyah, Iraq

Article Info

Article History:

Received 13 Oct 2025

Accepted 07 Jan 2026

Keywords:

Masonry wall;
Representative volume element;
Mortar joint thickness;
Concrete damage plasticity model;
Uniaxial compression

Abstract

In this study, the authors explore how the thickness of mortar joints has a significant impact on compressive behavior of the masonry of bricks in an integrated numerical modeling and experimental system. The joint thickness of masonry prism nine-course and joint thickness of 5mm, 10mm and 20mm were subjected to uniaxial compression tests. The results show that making the joint thicker i.e. 5mm to 20mm, compressive strength reduces by 34 % and the initial value of 3.5 MPa to 2.3 MPa, and initial elastic modulus decreases by 23 %. The middle area of the 9-course sample was verified as a Representative Volume Element (RVE), which was a successful way of eliminating border influences. Also, a micro modeling model of ABAQUS using the Concrete Damage Plasticity (CDP) model resulted in a high level of accuracy and the differences between experimental values of strength were limited to a range of 4.3 to 8.5%. These findings provide quantitative evidence supporting design code recommendations (e.g., ASTM C1314) to limit mortar bed joint thickness to 10 mm or less, thereby preserving the structural integrity and stiffness of masonry walls.

1. Introduction

Modern high-rise structures and innovative building technologies require accurate methods for calculating the stress-strain state of structures. This is particularly important for masonry, which exhibits significant structural heterogeneity due to the varying geometric and mechanical properties of bricks and mortar joints. Although brickwork exhibits high compressive strength, its low tensile strength often leads to cracking under loading conditions. This behavior must be carefully considered in design, especially when masonry is regarded as a load-bearing element in complex structures [1, 2].

The mechanical behavior of masonry is significantly influenced by the properties of its components, with mortar playing a key role. Recent studies have established that the mortar ratio and joint thickness are key parameters that determine compressive strength and shear resistance. Optimal load distribution is associated with 15 mm thick joints [5]; However, increasing the joint thickness above 20 mm leads to a reduction in structural integrity as a result of stress concentration [9]. These findings are consistent with previous studies on the influence of mortar type [7], effects at the brick-mortar interface [8], and the critical role of mortar strength in seismic performance [3, 4]. Despite these valuable findings, a systematic quantitative analysis of the effect of joint thickness in a practical range (e.g., 5–20 mm) coupled with a rigorously verified numerical model remains a gap in the literature.

[*]Corresponding author: majid.a.abdulhussein@qu.edu.iq
[a]orcid.org/0000-0002-3386-6463
DOI: http://dx.doi.org/10.17515/resm2026-1252me1013rs

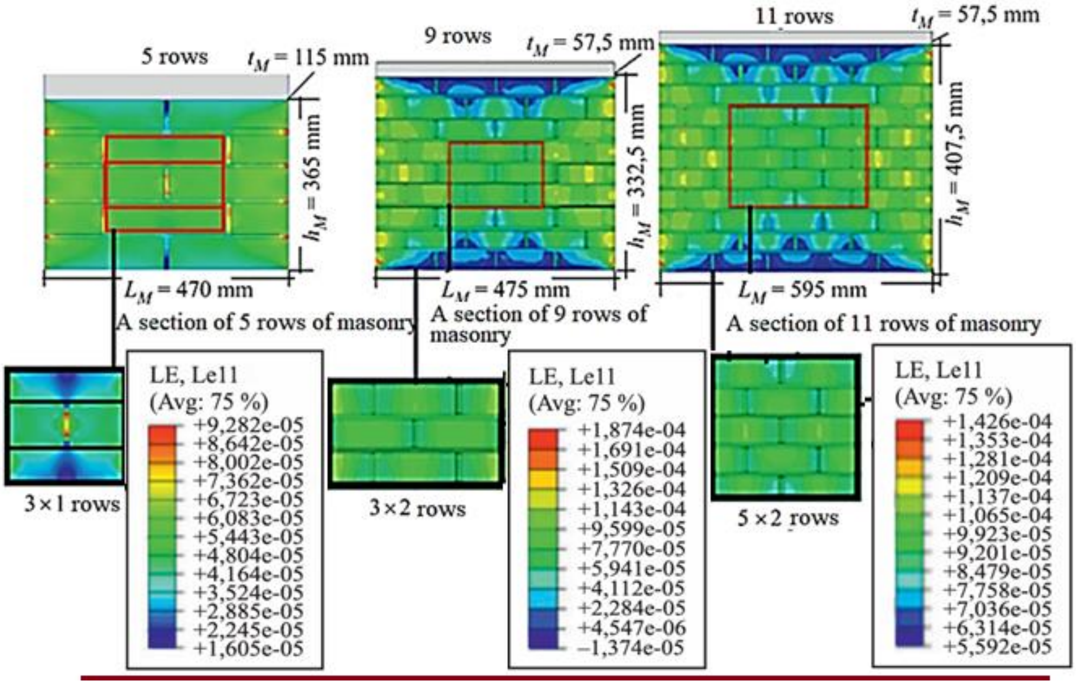

Fig. 1. Isofields of tensile strains in the horizontal direction for masonry of 5, 9, and 11 rows of bricks [1]

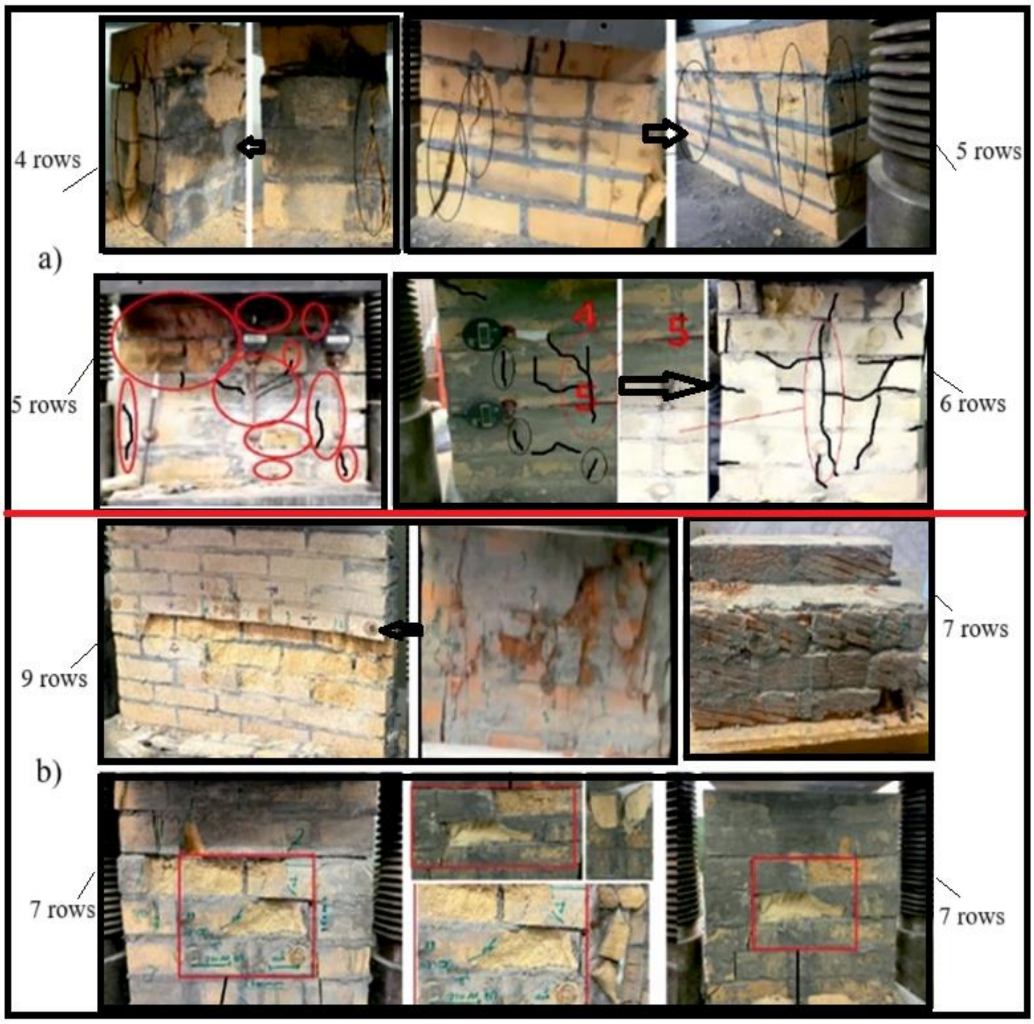

Fig. 2. Type of failure a– 4, 5, and 6 rows, b– 7 and 9 rows

A powerful approach to modeling such heterogeneous materials is multiscale homogenization based on the Representative Volume Element (RVE) [14]. RVE is the smallest volume of a material that effectively represents the overall macroscopic properties. For masonry, this means a fragment containing a sufficient number of bricks and mortar joints to capture the composite behavior while minimizing boundary effects. Consequently, a combined numerical-experimental study [1] justified the choice of a 9-course masonry fragment as a suitable RVE.

Finite element analysis of the strain fields under compression showed that the 9-course configuration minimizes boundary effects (in contrast to 5-course specimens) and ensures strain stabilization in the central zone (Fig. 1), which is confirmed by experimental strain measurements. Moreover, failure mechanism analysis [14, 15] confirmed that unreinforced 9-course masonry exhibits a representative failure pattern, including a combination of mortar damage and vertical cracking (Fig. 2), in contrast to smaller, non-representative specimens.

Independent experimental studies support the critical influence of specimen geometry on strain distribution, a key aspect of the RVE concept. It has been shown that lateral strains at mid-height of 1-meter-high walls are 3-4 times greater than at the boundaries, providing quantitative evidence of a significant strain gradient and the confinement effect exerted by loading platens [24]. The central zone is identified as the region representing true material behavior; accordingly, a 9-brick-high masonry fragment has been established as the minimum effective RVE in previous systematic studies [12, 13]. This size minimizes boundary effects, ensures strain stabilization in a central zone (approximately three bricks in height), and complies with code recommendations for deformation measurement bases. Thus, while smaller assemblies are used in practice, a 9-brick-high fragment is necessary to accurately characterize the macroscopic behavior of masonry under compression. Thus, despite existing research, there is a lack of studies that provide a systematic quantitative analysis of joint thickness effects across a practical range (5–20 mm) using an experimentally validated RVE-based micromodel. This study aims to fill this gap.

1.1 Novelty and Objectives of the Study

Based on these findings, this study fills the identified gap by providing a comprehensive experimental and numerical investigation of the effect of mortar joint thickness on the compressive behavior of masonry. The novelty of this work is threefold:

- Experimental Validation of the Methodology: Conducting a comprehensive experimental program on masonry fragments approved as RVE (9 courses) with systematically varied mortar joint thicknesses (5, 10, and 20 mm) to determine their compressive strength, elastic modulus, and deformation characteristics.
- Development and Verification of the Numerical Model: Developing a detailed micromodel in ABAQUS using the Concrete Damage Plasticity (CDP) model and rigorously validating it through direct comparison with the obtained experimental data for all joint thicknesses studied.
- Quantitative Analysis and Practical Recommendations: Conducting a direct quantitative comparative analysis of experimental and numerical results to assess the influence of mortar joint thickness and, based on this, formulating definitive, quantitative guidelines for optimal mortar joint thickness for design practice.

The goal of this study is to create a verified tool for numerical prediction and provide reliable, quantitatively substantiated recommendations for the design of high-performance masonry structures.

2. Materials and Methods

2.1 Materials

2.1.1. Brick Units

The clay bricks used in this study had standard Iraqi dimensions of 230 × 120 × 75 mm (length × width × height). Their physical and mechanical properties are summarized in Table 1.

2.1.2 Mortar

Ordinary Portland Cement (OPC) as a binder and local sand for the fine aggregate were used to prepare the mortar specimens. This mortar is notable for its strength, durability, and resistance to atmospheric and chemical deterioration. It is widely used for mortar and stucco work in stonework, block, and brick masonry. Mortar mix consisting of cement: sand proportions 1:3 was prepared manually. A total of nine specimens were fabricated, with a w/c ratio of 0.46 and mortar ratios: 1:3. The specimens were tested at 28 days. All specimens were cured in a controlled environment at a temperature of 22±2°C and relative humidity above 95% until testing. The procedures outlined in Fig. 3 were consistently followed throughout the study. The selection of specimen numbers followed the specifications outlined in ASTM C109.[23]. All properties are shown in Table 1.

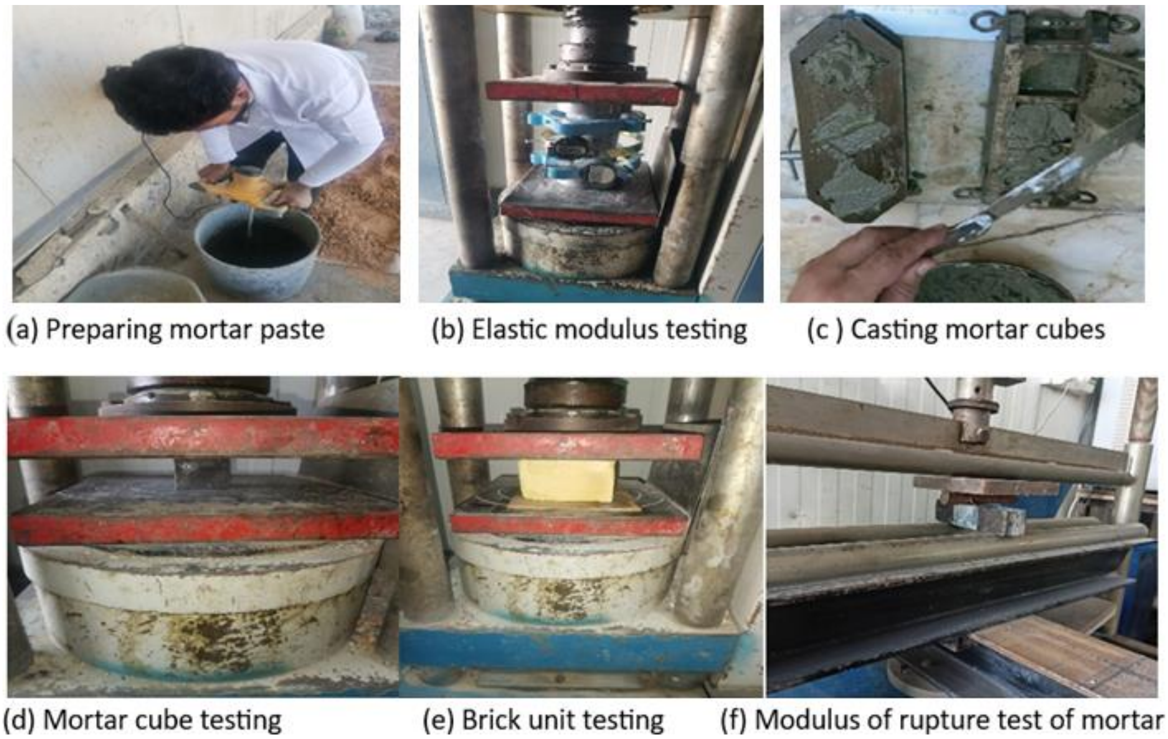

Fig. 3. Preparation and testing of mortar specimens (cube/cylinder)

Table 1. Physical and mechanical properties of constituent materials

Property	Mortar (1:3)	Masonry Unit (Brick)	Test Standard
Density (kg/m^3)	1850	1950	ASTM C642
Water Absorption (%)	8.0	8.5	ASTM C140
Compressive Strength (MPa)	5.0[1]	6.6[2]	ASTM C109 / EN 772-1
Flexural/Tensile Strength (MPa)	1.1	1.9	ASTM C348 / ASTM C67
Elastic Modulus (MPa)	4500	3750	ASTM C469

2.2 Methods

2.2.1 Sample Preparation

Masonry specimens were fabricated with three distinct mortar joint thicknesses: 5 mm, 10 mm, and 20 mm, applied uniformly to both bed (horizontal) and head (vertical) joints. For each thickness, two masonry walls were constructed using nine rows of standard bricks. The cross-sectional plan dimensions remained constant at 950 mm × 120 mm, while the total height varied due to the cumulative mortar joint thickness: 715 mm (5 mm joints), 755 mm (10 mm joints), and 835 mm (20 mm joints). Joint thickness was meticulously controlled to ensure uniformity.

Before construction, bricks were immersed in water for 24 hours to minimize water absorption from fresh mortar during curing. After immersion, bricks were arranged on a flat surface, and mortar was applied to achieve specified joint thicknesses. A stretcher bond pattern was used for wall assembly. Specimens were cured under controlled conditions for 28 days in accordance with standard cementitious curing practices (Fig. 4). A recognized limitation of this experimental campaign is the use of two specimens per configuration, which restricts detailed statistical analysis. However, the primary focus was on identifying clear trends and capturing failure mechanisms for subsequent numerical validation, a common approach in exploratory micromechanical studies.

Fig. 4. Construction and setup of walls to test

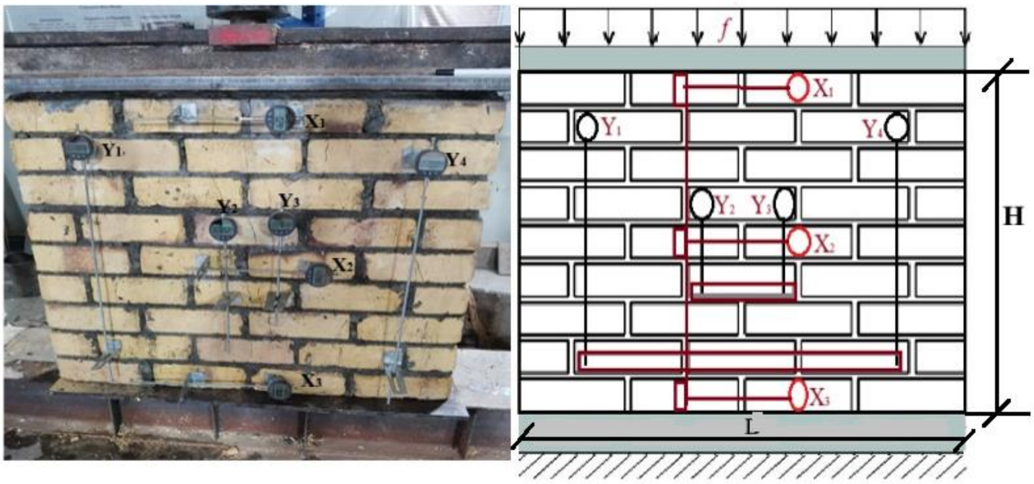

Fig. 5. General view of the compression test setup for masonry and the arrangement diagram of the instruments

2.2.2. Compressive Stress-Strain Test of The Specimen

Each specimen underwent uniaxial compression testing in a Universal Testing Machine (UTM) to determine its compressive strength and mechanical response of the masonry. The loads applied to the specimens were increased, and the strain at each level of 10 kN was measured with dial gauges with a measurement accuracy of 0.01 mm. The longitudinal and lateral strains were recorded at the same locations in the central parts of the masonry walls, which is equal to the representative volume element (RVE), and at the peripheries, which is equal to the boundary zones. Figure 5 gives a general illustration of the experimental situation, giving the geometrical features of the brickwork samples and showing a schematic of the measuring device. Each of the given mortar joint thicknesses was tested on six specimens, two specimens in each thickness increment. All the specimens were tested on compressive strength through measuring the highest load before it failed. To define the mechanical response and failure mode of the masonry walls during axial loading, the resulting stress strain trajectories of the individual mortar joint thicknesses were discussed to explain the behavior of the masonry walls.

At each stage of loading, the average relative elongations (deformations) in vertical and horizontal directions are calculated from the readings of the gauges(sensors) according to the formulas

$$\varepsilon_x = \frac{\Delta_x}{b_x}, \varepsilon_y = \frac{\Delta_y}{b_y} \tag{1}$$

Analogous to the elastic constants of a homogeneous material, we introduce the initial deformation modulus of the masonry E_0:

$$E_0 = \frac{F_y}{\varepsilon_y A} \tag{2}$$

Compressive strength of an individual tested samplef_k, was calculated using the formula:

$$f_k = \frac{f_{fai}}{A} \tag{3}$$

Table 3 presents the physical and mechanical properties obtained from the brick material tests.

2.3. Numerical Modeling Framework

To complement the experimental study, a detailed three-dimensional finite element (FE) micromodel was developed in ABAQUS/Explicit. The modeling strategy aimed to explicitly represent the heterogeneous structure of masonry, capturing the interaction between bricks and mortar joints.

2.3.1. Micro Modeling Approach and Geometry

The masonry walls were modeled brick-by-brick with explicit representation of bed (horizontal) and head (vertical) mortar joints. Bricks and mortar were discretized using 8-node linear brick elements with reduced integration (C3D8R). A mesh sensitivity study was conducted, leading to an optimal global element size of 10 mm, which ensured result convergence, particularly in the critical RVE zone, while maintaining computational efficiency. Convergence was considered achieved when the difference in predicted peak load between successive mesh refinements (e.g., 15 mm, 10 mm, 7 mm global size) was less than 2%. The interaction between brick and mortar was simulated using a surface-based cohesive contact formulation. A "hard" contact property governed the normal direction, preventing penetration.

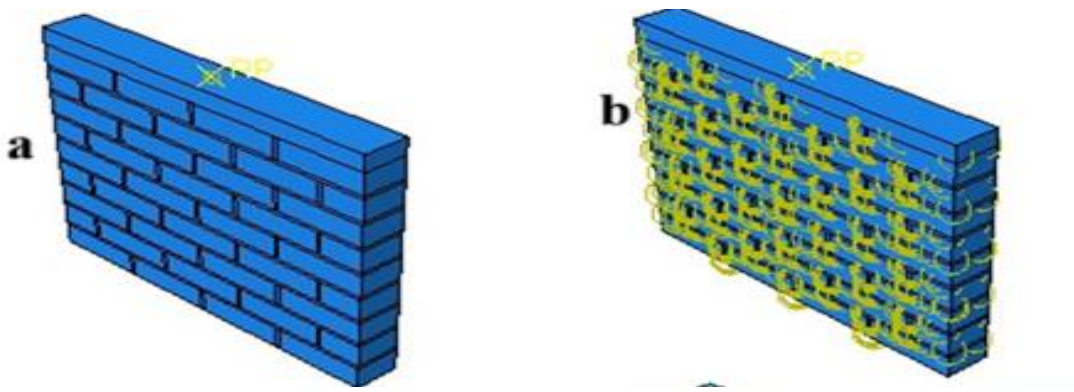

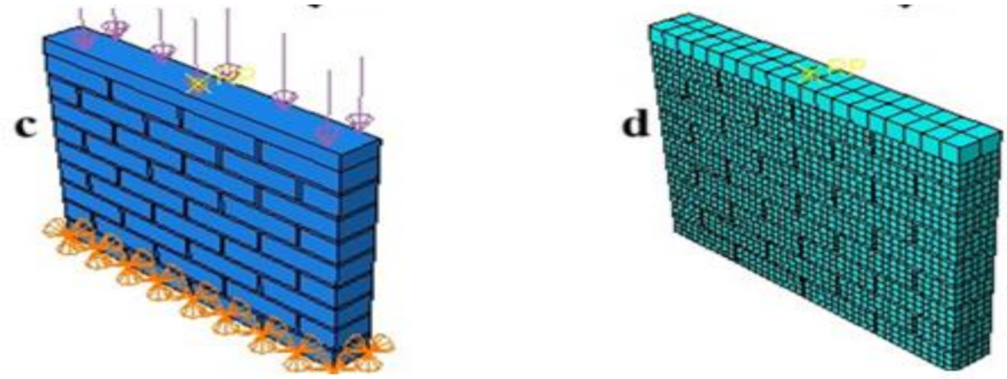

Fig. 6. Finite element methodology design for reinforced masonry: a) micromodel, b) behavior of base cohesive, c) masonry load, d) mesh

In the tangential direction, a Coulomb friction model with a coefficient of μ = 0.7 was adopted to model shear transfer and potential sliding. [17, 18, 20]. Loading was applied via an analytical rigid plate in displacement control, replicating the experimental setup and ensuring uniform displacement at the top of the specimen (Fig. 6). The bottom surface of the model was constrained against all translations and rotations, simulating the fixed support condition of the experimental test setup.

2.3.2. Material Constitutive Model and Calibration

The nonlinear behavior of both brick and mortar was simulated using the Concrete Damage Plasticity (CDP) model in ABAQUS [18, 20, 21]. This model is suitable for quasi-brittle materials as it captures stiffness degradation under both tensile (cracking) and compressive (crushing) failure modes through damage variables d_t, and d_c.

The core of the model implementation lies in defining the post-elastic stress-strain relationships. The uniaxial compressive stress is expressed as a function of inelastic strain ε_c^{in} and the compressive damage variable d_c:

$$f_c = (1 - d_c)E_0(\varepsilon_c - \varepsilon_c^{Pl}) \tag{4}$$

where E_0 is the initial elastic modulus, and ε_c^{pL} is the plastic strain derived from the inelastic strain [19]:

$$\varepsilon_c^{pL} = \varepsilon_c^{in} - \frac{dc}{(1 - d_c)}\frac{f_c}{E_0} \tag{5}$$

The damage variable d_c evolves from 0 (undamaged) to <1 and is directly related to the stress in the softening branch:

$$d_c = 1 - \frac{f_c}{f_{cu}} \ ,(0 \leq dc < 1) \tag{6}$$

where f_{cu} is the ultimate (peak) compressive strength. Analogous formulations with tensile damage, $d_t$govern behavior under tension [21].

Model calibration was performed in two steps. First, the CDP parameters for brick and mortar as standalone materials were calibrated by simulating uniaxial compression tests on their respective standard specimens (cubes/cylinders). The input parameters—compressive strength (f_c, f_{cu}), tensile strength (f_t), elastic modulus (E_0), and Poisson's ratio (ν)—were taken from the experimentally determined values in Table 1. The inelastic stress-strain curves defining the post-peak softening for each material were derived from these experimental data.

Second, the key plasticity parameters governing the yield surface and flow rule in the CDP model were selected based on established literature for masonry constituents [25, 26, 29] and are summarized in Table 2. The dilation angle (ψ=10°) and eccentricity (ϵ=0.1) were kept identical for both materials to ensure numerical stability. The default values for the biaxial-to-uniaxial compressive strength ratio (f_{b0}/f_{c0}=1.16) and the shape parameter K_c (0.667 for mortar, 0.7 for brick) were adopted, as they provided the best fit to the experimental load-displacement response of the full masonry walls during initial model tuning.

Table 2. Plasticity parameters for brick and mortar at masonry failure

Plasticity Parameter	Materials for masonry	
	Brick	Mortar
Dilation Angle, (ψ)	10°	10°
Flow Potential Eccentricity (ϵ)	0.1	0.1
Biaxial/Uniaxial Comp. Ratio, (f_{b_0} / f_{c_0})	1.16	1.16
Yield Surface Shape Parameter, (k)	0.7	0.667
Viscosity Parameter, (ν)	0.0001	0.0001

3. Results and Discussion

3.1. Validation of Representative Volume Element (RVE) through Strain Analysis

The experimental strain data, recorded via seven indicators (four vertical: Y_1-Y_4; three horizontals: X_1-X_3), revealed the heterogeneous nature of masonry under compression. A clear strain gradient was observed from the specimen boundaries to its center. The readings from indicators Y_1 and Y_4 (edge zones) and X_1 and X_3 showed minimal and statistically insignificant variation, indicating constrained deformation near the loading platens due to the "platen restraint effect" [17, 22].

In contrast, indicators Y_2, Y_3 (vertical), and X_2 (horizontal), positioned in the central section, recorded substantially higher strain values (Table 3). This central zone exhibited stabilized strains, relatively free from the direct influence of boundary conditions. This pattern confirms the formation of a region with a representative and uniform stress-strain state, justifying its designation as the Representative Volume Element (RVE) for homogenization analysis. These results are in full agreement with established findings that maximum deformations in masonry prisms occur at mid-height, with central strains being 3-4 times greater than those at the top and bottom due to end restraints [17, 24].

The successful isolation of this stabilized central zone within the 9-row specimen validates its sufficiency as an RVE. Smaller configurations (e.g., 5 rows) are dominated by boundary effects, preventing the development of a representative stress field, while the 9-row fragment provides the necessary height for stress redistribution and the establishment of a characteristic deformation kernel.

Table 3. Experimental values of transverse and longitudinal deformations

Masonry wall		$\varepsilon_{y1,4}$	$\varepsilon_{y2,3}$ RVE zone	$\varepsilon_{x1,3}$	RVEon ε_{x2}
Type 1	1	-0.00016	-0.00028	0.000045	0.00021
	2	-0.00021	-0.00036	0.000051	0.00027
Average Value		-0.00018	-0.00032	0.000048	0.00024
Std. Dev.		0.000035	0.000057	0.000004	0.000042
Type 2	1	-0.000159	-0.00082	0.000092	0.00033
	2	-0.000360	-0.00086	0.000170	0.00039
Average Value		-0.000260	-0.00084	0.000130	0.00036
Std. Dev.		0.000142	0.000028	0.000055	0.000042
Type 3	1	-0.000192	-0.001400	0.000350	0.00100
	2	-0.000390	-0.001700	0.000580	0.00130
Average Value		-0.000290	-0.001500	0.000460	0.00110
Std. Dev.		0.000140	0.000212	0.000162	0.000212

Note: Std. Dev. = Standard Deviation, calculated from two specimens per joint thickness, indicating the scatter in measured values. Lower values suggest better reproducibility

3.2. Quantitative Influence of Mortar Joint Thickness on Mechanical Behavior

The compressive strength and deformation characteristics of masonry are critically dependent on mortar joint thickness, as summarized in Tables 3 and 4. The analysis reveals a pronounced trend: increasing joint thickness from 5 mm to 20 mm significantly degrades structural performance.

- Compressive Strength: The average compressive strength decreased by 20% (from 3.5 MPa to 2.8 MPa) when joint thickness increased from 5 mm to 10 mm, and by a further 18% (to 2.3 MPa) when increased to 20 mm, resulting in a total reduction of 34%. The ratio of cracking load to failure load ($\frac{F_{cr}}{F_{fr}}$) also decreased from 0.256 to 0.2, indicating that masonry with thicker joints enters the nonlinear, damaging phase at a lower proportion of its ultimate capacity.
- Stiffness: The initial elastic modulus (E_0) showed a consistent decline, dropping by 12**%** (from 11,128 MPa to 9,750 MPa) and then 13% (to 8,525 MPa) for the 10 mm and 20 mm joints, respectively. This 23% total reduction signifies a substantial loss in global stiffness, making the structure more susceptible to deformation under service loads.
- Deformation Capacity: Conversely, the deformation capacity, particularly in the transverse direction, increased dramatically. The average transverse strain in the RVE zone (ε_{x2}) amplified by approximately 50% (from 0.00024 to 0.00036) and then 300**%** (to 0.0011) for the 10 mm and 20 mm joints, respectively, compared to the 5 mm baseline.
- Mechanistic Interpretation: This behavior stems from the changing role of the mortar layer. In thin joints (5 mm), the mortar acts as a stiff, high-confinement binder, facilitating efficient load transfer and forcing a brittle, brick-dominated tensile failure. As thickness increases, the mortar volume creates a more compliant, weak interface. This layer undergoes greater shear and compressive plastic deformation, leading to stress concentration, reduced composite action, and a transition to a mortar-dominated, quasi-plastic failure mode. The non-linear relationship—where a 400% increase in transverse strain corresponds to a 34% strength loss—highlights this fundamental shift in the failure-controlling phase from brick to mortar.

The standard deviations (SD) presented in Table 4 indicate the scatter of the experimental data. The relatively low values of standard deviation for the mechanical properties (particularly for the compressive strength f_i and elastic modulus E_0) confirm good reproducibility of the results even with the limited number of specimens (n=2 per joint thickness). However, it should be noted that the small sample size restricts the possibility of conducting a comprehensive statistical analysis, and the obtained results primarily demonstrate clear qualitative trends of the joint thickness influence. This mechanistic shift is accurately captured by the CDP model in the numerical simulation, where the damage variable (d) develops more rapidly and extensively within the thicker mortar joints (see Section 4.3).

Table 4. Strength characteristics of masonry under uniaxial compression

Masonry wall		f_i (MPa)	F_{fr} (kN)	F_{cr} (kN)	$\frac{F_{cr}}{F_{fr}}$	E_0 (MPa)
Type1	1	3.7	431	120	0.278	11406.22
	2	3.3	466	110	0.236	10850.40
Average Value		3.5	448	115	0.256	11128.3
Standard deviation (SD)		0.283	24.75	7.07	0.030	393
Type2	1	2.9	350	80	0.228	9 500
	2	2.7	330	77	0.233	10000
Average Value		2.8	340	78.5	0.230	9750
Standard deviation (SD)		0.141	14.14	2.12	0.004	354
Type3	1	2.2	280	50	0.178	8700
	2	2.3	295	65	0.220	8350
Average Value		2.3	287	57.5	0.2**00**	8525
Standard deviation (SD)		0.071	10.61	10.61	0.030	247

The standard deviation (SD) values indicate good reproducibility despite the limited sample size (n=2 per configuration). For validation, the numerical model showed deviations of 8.5%, 7.0%, and 4.3% for 5 mm, 10 mm, and 20 mm joints, respectively. The coefficient of determination (R^2) exceeded 0.98 for all cases, and the root mean square error (RMSE) was below 0.15 MPa, confirming high predictive accuracy.

3.3. Analysis of Stress-Strain Response and Failure Modes

The stress-strain curves for each joint thickness (Figs. 7-9) provide further insight into the evolving mechanical response.

- 5 mm Joint (Fig. 7): The response is predominantly linear-elastic until near peak load, with a sharp post-peak drop, characteristic of brittle fracture. The significant strain difference between the central RVE and edge zones underscores the effectiveness of the 9-row setup in mitigating boundary effects for homogenization.
- 10 mm Joint (Fig. 8): Increased nonlinearity is evident, especially beyond 50-60% of peak stress. This represents progressive damage accumulation within the mortar joints. The strain gradient between the center and edges persists but is less pronounced than in the 5 mm case, indicating more distributed damage.
- 20 mm Joint (Fig. 9): The curve exhibits marked nonlinearity from the onset of loading, signaling immediate inelastic compaction and microcracking in the thick mortar beds. The overall response is more ductile-like (gradual softening), with failure governed by the crushing and shear failure of the mortar.

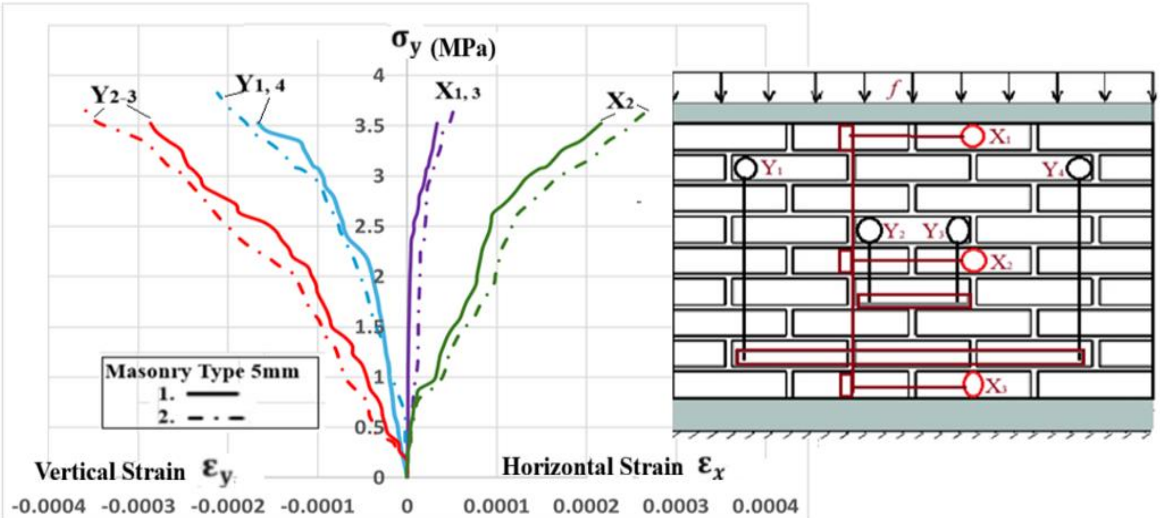

Fig. 7. Stress vs strain relationships for masonry with 5 mm mortar joints

3.4. Synthesis and Practical Implications

The integrated results demonstrate that mortar joint thickness is not merely a construction detail but a key design parameter controlling the composite behavior of masonry. The validated 9-row RVE provides a reliable basis for homogenized modeling. The quantitative relationships established here—linking joint thickness to strength, stiffness, and ductility offer valuable input for performance-based design.

From a practical standpoint, the sharp decline in performance beyond a 10 mm joint thickness is critical. For seismic-resistant design, where controlled energy dissipation is required, the limited benefit of increased deformation capacity with 20 mm joints is far outweighed by the severe penalty in strength and stiffness. Therefore, based on this evidence, limiting mortar bed joint thickness to 10 mm or less is recommended in design codes and specifications for load-bearing masonry, particularly in mid- to high-rise construction. This recommendation aligns with the upper limits suggested in best practice guides [22] and ensures optimal utilization of the brick masonry's inherent compressive strength. Increased nonlinearity indicates progressive damage in mortars. The central RVE zone experiences significantly higher strains.

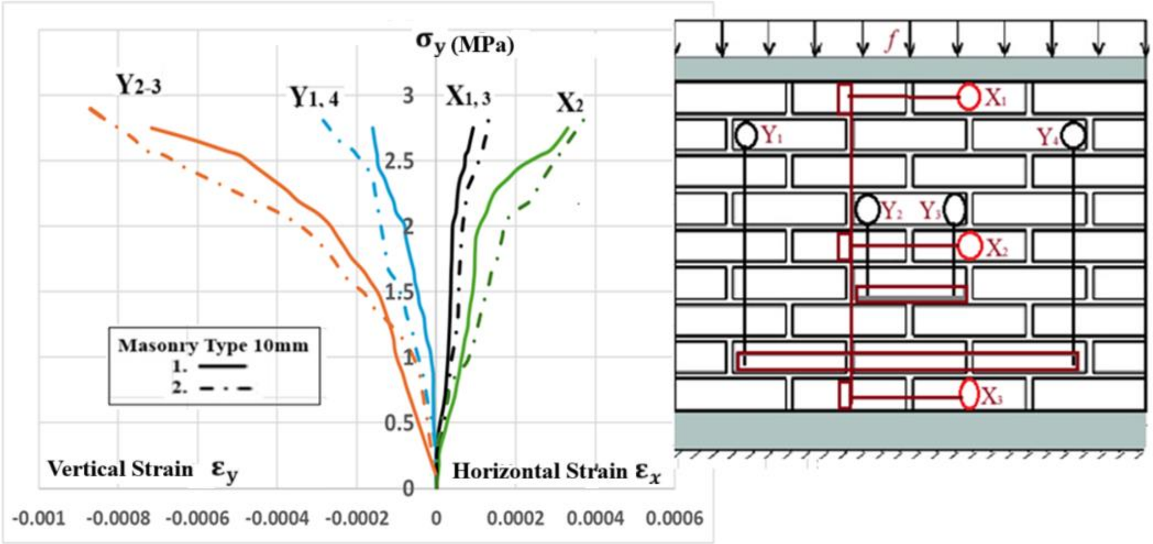

Fig. 8. Stress vs strain relationships for masonry with 10 mm mortar joints

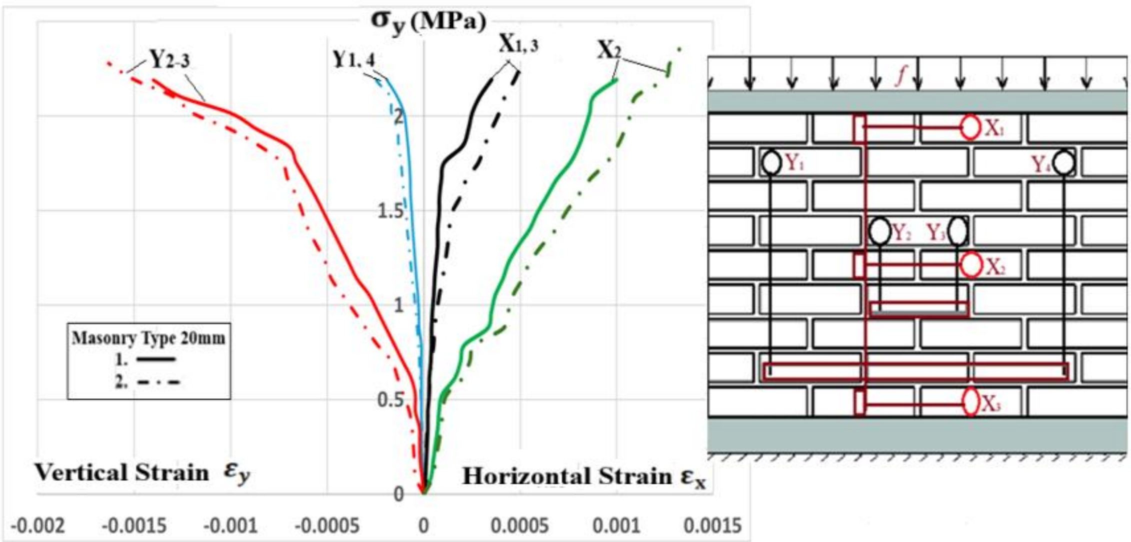

Fig. 9. Stress vs strain relationships for masonry with 20 mm mortar joints

4. Numerical Results and Validation

The validated numerical model successfully replicated the key experimental findings. Fig. 10 shows a direct comparison of the failure modes. For the 5 mm joint, both model and test exhibit vertical cracking in the central RVE. For the 20 mm joint, the model accurately predicts the shift to mortar-crushing failure.

Quantitative validation is presented in Fig. 11, comparing the experimental and numerical stress-strain curves. The model shows excellent agreement with the experimental compressive strength, with deviations of only 8.5%, 7.0%, and 4.3% for the 5 mm, 10 mm, and 20 mm joint thicknesses, respectively. The coefficient of determination (R^2) between the experimental and numerical stress-strain curves exceeded 0.98 for all cases. Furthermore, the model accurately captures the reduction in initial stiffness (E_0) and the increasing nonlinearity with thicker joints. The high degree of correlation (deviations < 9%, R^2 > 0.98) validates the chosen micro modeling approach and the calibration of the CDP parameters.

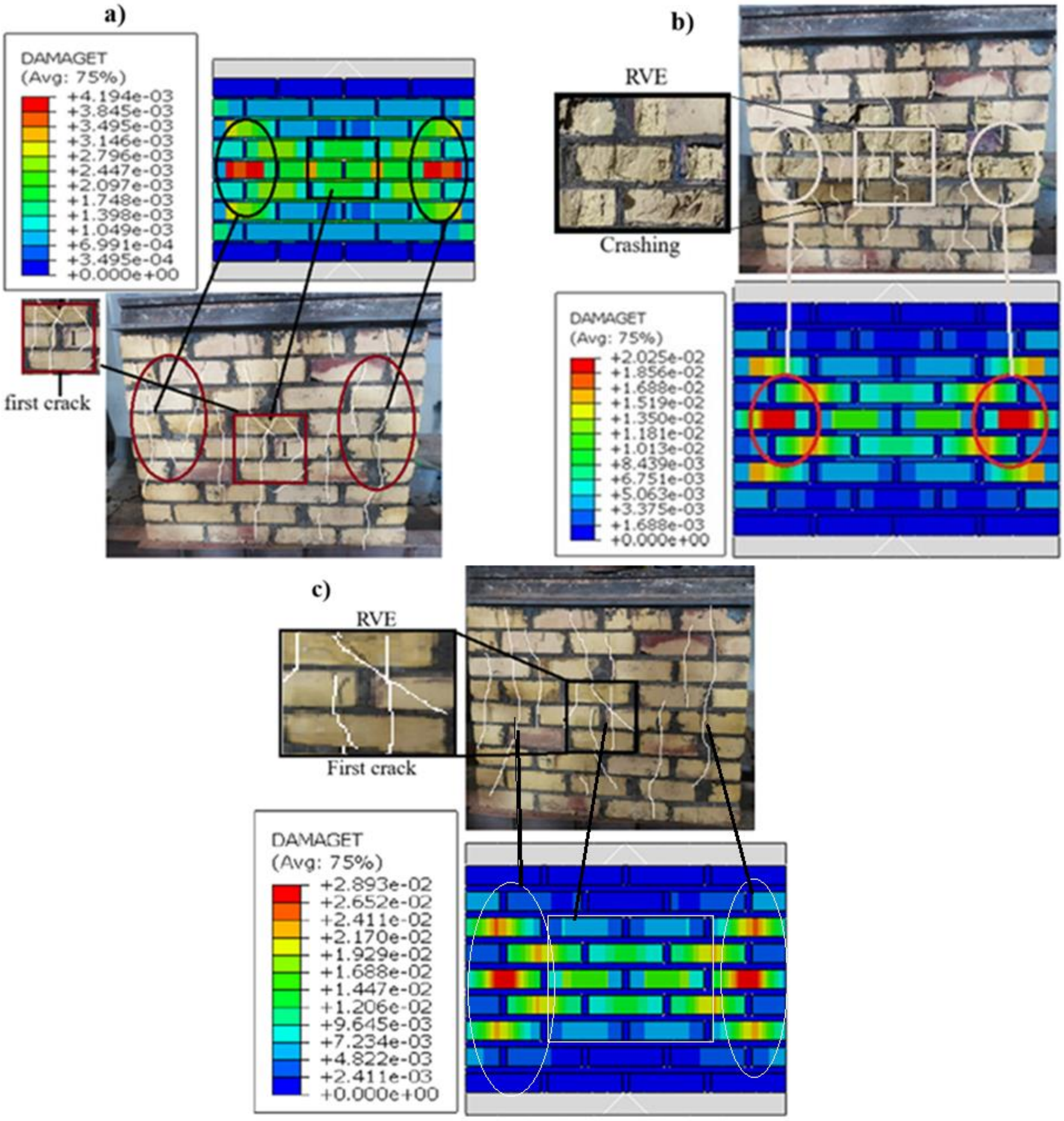

Fig. 10. Comparative analysis of masonry wall failure modes: Experimental vs. numerical simulation for (a) 5mm, (b) 10mm, and (c) 20mm mortar joint thicknesses

Quantitative validation is presented in Figure 11, comparing the experimental and numerical stress-strain curves. The model shows excellent agreement with the experimental compressive strength, with deviations of only 8.5%, 7.0%, and 4.3% for the 5 mm, 10 mm, and 20 mm joint thicknesses, respectively. Furthermore, the model accurately captures the reduction in initial stiffness (E_0) and the increasing nonlinearity with thicker joints.

The high degree of correlation (deviations < 9%) validates the chosen micro modeling approach, the calibration of the CDP parameters, and the overall numerical framework. This model can now be considered a reliable tool for predicting the compressive behavior of the studied masonry type under the investigated range of joint thicknesses.

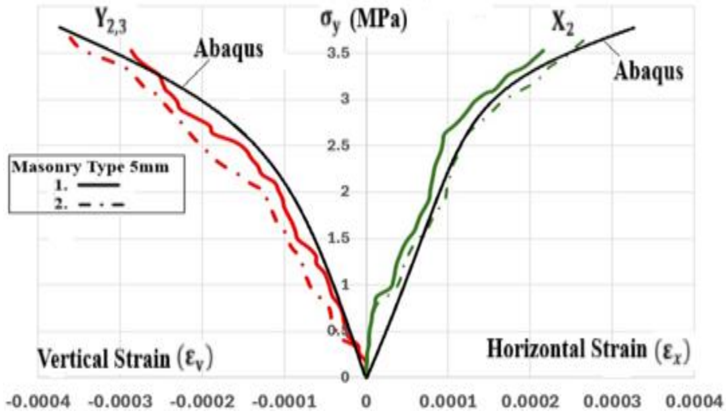

(a)

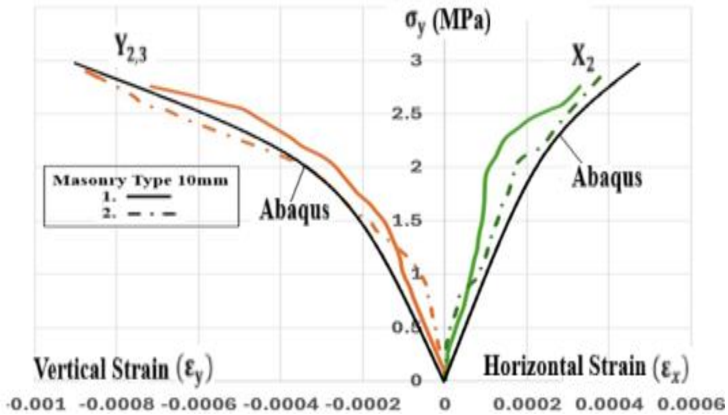

(b)

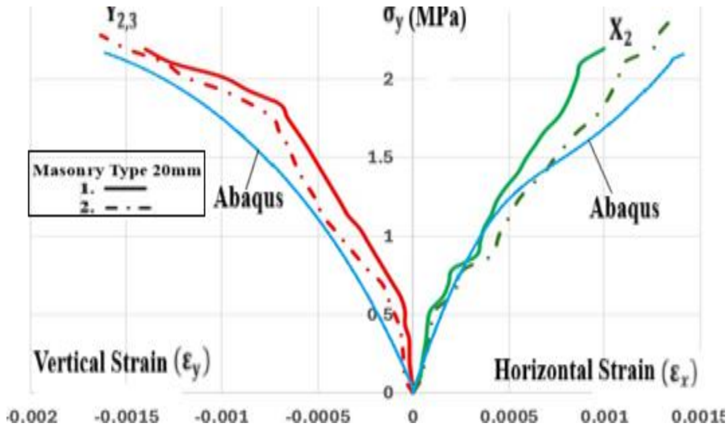

(c)

Fig. 11. Comparison and Validation of Numerical (ABAQUS) and Experimental Results for Mortar Joints with Thicknesses of (a) 5 mm, (b) 10 mm, and (c) 20 mm

5. Conclusions

This integrated experimental and numerical study investigated the influence of mortar joint thickness on the mechanical behavior of brick masonry. Based on the analysis of results, the following key conclusions can be drawn:

- Validation of RVE Configuration: The nine-row masonry fragment was rigorously validated as a Representative Volume Element (RVE) for the analysis of heterogeneous masonry. Experimental strain measurements confirmed that this configuration effectively minimizes boundary effects and ensures strain stabilization in the central zone, thus providing a reliable basis for determining homogenized mechanical properties and macro-modeling.

- Quantitative Impact of Mortar Joint Thickness: Mortar joint thickness was identified as a critical parameter governing the macroscopic mechanical response. A clear and quantifiable detrimental relationship was established: increasing the joint thickness from 5 mm to 20 mm resulted in a significant 34% reduction in compressive strength (from an average of 3.5 MPa to 2.3 MPa) and a 23% decrease in the initial elastic modulus (E_0 from 11,128 MPa to 8,525 MPa). Concurrently, transverse deformations in the RVE zone amplified by approximately 400%.
- Shift in Failure Mechanism: The increase in joint thickness precipitated a fundamental shift in the failure mode. For thin joints (5 mm), failure was characterized by brittle vertical cracking localized in the brick units of the central RVE zone, driven by tensile stresses from Poisson's effect. In contrast, for thick joints (20 mm), the failure transformed into a quasi-plastic mode dominated by crushing and shear damage within the mortar joints themselves, leading to a loss of structural integrity at lower stress levels.
- Reliability of Numerical Framework: The micro modeling approach in ABAQUS, utilizing the Concrete Damage Plasticity (CDP) model with carefully calibrated parameters, demonstrated high predictive fidelity. The model accurately replicated the experimental stress-strain responses and failure patterns across all joint thicknesses, with deviations in compressive strength of less than 8.5%. This validates the numerical framework as a robust tool for the virtual analysis and design of similar masonry systems.
- Practical Implications and Recommendations: For optimal structural performance, particularly in contexts requiring high load-bearing capacity or seismic resistance (e.g., high-rise or critical infrastructure), the findings mandate a strict control of mortar joint thickness. Based on the sharp decline in performance beyond 10 mm, it is recommended that the mortar joint thickness in design and construction practice should not exceed 10 mm to preserve strength, stiffness, and a favorable brittle failure mode. This recommendation supports and quantifies the prudent limits often suggested in best practice guides and provides a technical basis for code specifications (e.g., the emphasis on thin joints in ASTM C1314 for prism testing).
- Study Limitations and Future Work: The conclusions are derived from a specific brick type and mortar mix, with a limited number of specimens per configuration. Future research should expand the statistical basis and investigate the interaction of joint thickness with other variables, such as mortar strength, brick geometry, and reinforcement, under more complex loading scenarios (e.g., cyclic, shear). The validated numerical model presented here provides a solid foundation for such parametric studies.

References

[1] Adishchev VV, Shakarneh OMD. Identification of effective stiffness characteristics of masonry based on comparative analysis results of numerical and physical experiments. News of Higher Educational Institutions. Construction. 2024;8:5-21. https://doi.org/10.32683/0536-1052-2023-771-3-5-21
[2] Adishchev VV, Shakarnekh OMD. The effect of reinforcement on the physical and mechanical characteristics of masonry of ceramic blocks. News of Higher Educational Institutions. Construction. 2022;5:14-30. https://doi.org/10.32683/0536-1052-2022-761-5-14-30
[3] El-Dakhakhni MA, El-Sheikh MA. Influence of mortar properties on the seismic behavior of masonry walls. Journal of Building Engineering. 2021;28:101724.
[4] Haach VG, Vasconcelos G, Lourenço P, Mohamad G. Influence of the mortar on the compressive behavior of concrete masonry prisms. Revista da Associação Portuguesa de Análise Experimental de Tensões. 2010;18:79-84.
[5] Jadhav S, Awardi G, Yeri S. Influence of mortar strength and thickness on the mechanical characteristics of masonry brickwork. Journal of Systems Engineering and Electronics. 2021;31(1):265-277.
[6] Jagadish K, Shetty GK, Nayak GU. Effect of mortar mix on compressive strength of brickwork. International Journal of Applied Engineering Research. 2016;11(5):3129-3134.
[7] Liang B, Zhang H, Liu Z, Hou J. The influence of different types of mortar on the compressive strength of masonry. Journal of Building Engineering. 2023;65:105635. https://doi.org/10.1016/j.jobe.2022.105635

[8] Sarhosis V, Garrity SW, Sheng Y. Influence of brick-mortar interface on the mechanical behaviour of low bond strength masonry brickwork lintels. Engineering Structures. 2015;88:1-11. https://doi.org/10.1016/j.engstruct.2014.12.014
[9] Usman M, Panwar R. The influence of mortar thickness and strength on the mechanical characteristics of masonry brickwork. International Journal of Progressive Research in Engineering Management and Science. 2024;4(5):1775-1783.
[10] Zengin B. The effect of the bricks used in masonry walls on characteristic properties. Sigma Journal of Engineering and Natural Sciences. 2017;35(4):667-677.
[11] Ghiassi B, Milani G. Numerical modeling of masonry and historical structures: From theory to application. London: Woodhead Publishing; 2019. (Woodhead Publishing Series in Civil and Structural Engineering).
[12] Shakarneh OMD. Homogenization method for determining the matrix of effective stiffness coefficients of reinforcement masonry wall. Trudy NGASU = Proceedings of the Novosibirsk State University of Architecture and Civil Engineering. 2024;27(4).
[13] Adishchev VV, Shakarneh OMD. Determination of the physical characteristics of masonry based on a structural approach. News of Higher Educational Institutions. Construction. 2025;4:32-44.
[14] Shakarneh OMD. Main mechanisms of masonry failure as a structurally heterogeneous material. News of Higher Educational Institutions. Construction. 2025;6:31-43.
[15] Adishchev VV, Shakarneh OMD. Processes of elastic and inelastic deformation and destruction of stone masonry. News of Higher Educational Institutions. Construction. 2025;2:5-18.
[16] Hermoune H, Benabed B, Alshugaa M, Abousnina R, Guettala A. Strengthening of masonry walls with CFRP composite: Experiments and numerical modeling. Építôanyag - Journal of Silicate Based and Composite Materials. 2020;72(1):2-11. https://doi.org/10.14382/epitoanyag-jsbcm.2020.1
[17] Kaushik HB, Rai DC, Jain SK. Stress-strain characteristics of clay brick masonry under uniaxial compression. Journal of Materials in Civil Engineering. 2007;19(9):728-739. https://doi.org/10.1061/(ASCE)0899-1561(2007)19:9(728)
[18] Lee J, Fenves G. Plastic-damage model for cyclic loading of concrete structures. Journal of Engineering Mechanics. 124(8):892-900. https://doi.org/10.1061/(ASCE)0733-9399(1998)124:8(892)
[19] Lourenco PB. Computational strategies for masonry structures [PhD thesis]. Delft: Delft University of Technology; 1996.
[20] Lubliner J, Oliver J, Oller S, Onate E. A plastic-damage model for concrete. International Journal of Solids and Structures. 1989;25(3):299-326. https://doi.org/10.1016/0020-7683(89)90050-4
[21] Milani G, Valente M, Alessandri C. The narthex of the Church of the Nativity in Bethlehem: A non-linear finite elements approach to predict the structural damage. Computers and Structures. 2018;207:3-18. https://doi.org/10.1016/j.compstruc.2017.03.010
[22] European Committee for Standardization. EN 1052-1:2009 - Methods of test for masonry. Part 1: Determination of compressive strength. Brussels: European Committee for Standardization; 2009.
[23] ASTM International. ASTM C109-14: Standard test method for compressive strength of hydraulic cement mortars (using 2-in. or 50-mm cube specimens). West Conshohocken, PA: ASTM International; 2014.
[24] Fonseca FS, Mohamad G, Roman HR, Vermeltfoort A, Rizzatti E. Deformation and failure mode of masonry. In: 12th North American Masonry Conference; 2015 May 17-20; Denver, Colorado. p. 1-12.
[25] Mousavi R, Champiri MD, Willam KJ. Efficiency of damage-plasticity models in capturing compaction-expansion transition of concrete under different compression loading conditions. Proceedings of the 7th European Congress on Computational Methods in Applied Sciences and Engineering. 2016;172:1-12. https://doi.org/10.7712/100016.1810.12018
[26] Genikomsou AS, Polak MA. Finite element analysis of punching shear of concrete slabs using damaged plasticity model in ABAQUS. Engineering Structures. 2015;98:38-48. https://doi.org/10.1016/j.engstruct.2015.04.016
[27] Dassault Systèmes. ABAQUS user's guide (Version 6.13). Providence, RI: Dassault Systèmes Simulia Corp; 2013.
[28] Wang SY, Sloan SW, Abbo AJ, Masia MJ, Tang CA. Numerical simulation of the failure process of unreinforced masonry walls due to concentrated static and dynamic loading. International Journal of Solids and Structures. 2012;49(2):377-394. https://doi.org/10.1016/j.ijsolstr.2011.10.016